JOURNAL OF MATERIALS SCIENCE: MATERIALS IN MEDICINE **16** (2005) 213–219

Preparation and *in vitro* investigation of chitosan/nano-hydroxyapatite composite used as bone substitute materials

ZHANG LI, LI YUBAO*, YANG AIPING, PENG XUELIN, WANG XUEJIANG, ZHANG XIANG
Research Center for Nano-Biomaterials, Analytical & Testing Center, Sichuan University, Chengdu 610064, People's Republic of China
E-mail: nic7504@scu.edu.cn

Chitosan/nano-hydroxyapatite composites with different weight ratios were prepared through a co-precipitation method using $Ca(OH)_2$, H_3PO_4 and chitosan as starting materials. The properties of these composites were characterized by means of TEM, IR, XRD, burn-out test and universal matertial test machine. Additionally, *in vitro* tests were also conducted to investigate the biodegradability and bioactivity of the composite. The results showed that the HA synthesized here was poorly crystalline carbonated nanometer crystals and dispersed uniformly in chitosan phase and there is no phase-separation between the two phases. Because of the interactions between chitosan and n-HA, the mechanical properties of these composites were improved, and the maximum value of the compressive strength was measured about 120 MPa corresponding to the chitosan/n-HA composite with a weight ratio of 30/70. The specimens made of 30/70 chitosan/n-HA composite exhibit high biodegradability and bioactivity when being immersed in SBF solutions. The composite is appropriate to being used as scaffold materials for bone tissue engineering.

1. Introduction

Hydroxyapatite (HA) has been extensively investigated due to its excellent biocompatibility, bioactivity and osteoconductivity as well as its similarities to the main mineral component of bone [1–4]. However, the poorly compressive strength and fatigue failure limit its applicability to the low or non load-bearing sites in human body. Additionally, it has been reported that HA in the form of powders, used for the treatment of bone defects, has problem associated with migration to places other than implanted areas [5, 6]. As we know, various biocomposites existing in nature, such as shells and pearls, are all organic/inorganic composites with good mechanical properties, which may provide a route to resolve the above problems. Extensive research has been carried out in this regard and composite materials based on HA and a variety of polymers have been worked out [7–10].

Chitosan, a natural biodegradable polymer, is a low acetyl substituted form of chitin named (1-4)-2-amino-2-deoxy-(D-glucose). Because of its unique properties such as biodegradability, nontoxicity, anti-bacterial effect and biocompatibility, much attention has been paid to chitosan-based biomedical materials [11–15]. However, lack of bone-bonding bioactivity limits its use in bone tissue engineering. Therefore, it is desirable to develop a composite material with favorable properties of chitosan and hydroxyapatite. The designed composites are expected to have an optimal mechanical performance and a controllable degradation rate as well as eminent bioactivity and this will be of great importance for bone remodeling and growth.

In the system of $Ca(OH)_2$-H_3PO_4-H_2O, HA is the most basic calcium orthophosphate [16], this compound is therefore insoluble in neutral and basic medium. The precipitation PH of chitosan is generally more than 6.0 [17]. That is to say, the conditions for both HA and chitosan to precipitate are almost the same. These properties enable the precipitation of a chitosan-HA composite material. Therefore, a series of chitosan/n-HA composites in this study were prepared through a co-precipitation method.

In order to investigate the bioactivity and the biodegradability of chitosan/n-HA composites, the *in vitro* experiment of the 30/70 chitosan/n-HA composite immersed in a simulated body fluid (SBF) was also conducted.

*Author to whom all correspondence should be addressed.

TABLE I The dosage of reagents for the preparation of chitosan/n-HA composites (20 g product)

Chitosan/n-HA composite (weight ratio)	Chitosan (g)	H_3PO_4 (g)	$Ca(OH)_2$ (g)
0/100	0	11.71	14.76
20/80	4	9.37	11.81
30/70	6	8.20	10.33
40/60	8	7.03	8.86
50/50	10	5.86	7.38
60/40	12	4.69	5.90
70/30	14	3.51	4.43

2. Materials and methods

2.1. Preparation of chitosan/n-HA composites

An 80-mesh chitosan powder was purchased from Haidebei bioengineering Co. Ltd., JiNan, China, with a molecular weight of about 250,000 and an *N*-deacetylation degree of 80%. Calcium hydroxide, phosphoric acid and all other reagents used in the present study were of analytical grade. Calcium hydroxide was screened through a 200-mesh sieve before used.

The chitosan/n-HA composites were synthesized by the following procedure. Chitosan solution with a concentration of 3 wt% was prepared by dissolving chitosan into 2 wt% acetic acid with stirring for 5 h to get a perfectly transparent solution. Then, a 10 wt% solution of H_3PO_4 was mixed with the chitosan solution. The starting content of these reagents were scaled according to the final chitosan/n-HA weight ratios of 0/100, 20/80, 30/70,40/60, 50/50, 60/40, 70/30, and the initial amount of these reagents used here were listed in Table I. The mixed chitosan/H_3PO_4 solution was then dropped slowly into the 4% ethanol solution of calcium hydroxide with vigorous stirring and the PH was adjusted with NaOH solution to about 10. The dropping speed was near 4 ml min^{-1} and the reaction was carried out in ambient condition. After titration, the stirring was kept for 24 h, then the obtained slurry was aged for another 24 h. Finally, the precipitate was filtered, and washed with deionized water and dried in a vacuum oven at 80 °C.

2.2. Characterization of chitosan/n-HA composites

The uniformity of these composites was measured by burn-out test at 800 °C. The microstructure of n-HA and chitosan/n-HA composites was observed with a transmission electron microscope (TEM), the crystal structure of n-HA, chitosan and their composites was determined by X-ray diffractometry (XRD) and infrared spectroscopy (IR).

The chitosan/n-HA powder was adjusted into paste with citric acid solution and then was mould into a clava, which was then immersed into a coagulant for 3 h. After then dried in air, the clava was processed into a rod with a size of $\Phi 6 \times 12$ mm for mechanical test. Compressive strength were determined using a Universal testing machine at a crosshead of 1 mm/min.

TABLE II Ionic concentrations of SBF in comparison with those of human blood plasma

	Concentration (mM)							
	Na^+	K^+	Ca^{2+}	Mg^{2+}	HCO_3^-	Cl^-	HPO_4^{2-}	SO_4^{2-}
Blood plasma	142.0	5.0	2.5	1.5	27.0	103.0	1.0	0.5
SBF	142.0	5.0	2.5	1.5	4.2	148.0	1.0	0.5

2.3. *In vitro* tests

SBF solution, in which ionic concentrations were shown in Table II, was prepared by dissolving reagent-grade NaCl, $NaHCO_3$, KCl, $K_2HPO_4 \cdot 3H_2O$, $MgCl_2 \cdot 6H_2O$, $CaCl_2$, and Na_2SO_4 in deionized water. The solution was buffered at PH 7.4 with tris(hydroxymethyl) aminomethane ($(CH_2OH)_3CNH_2$) and 1M hydrochloric acid (HCl) at 36.5 °C. 10 wt% citric acid solution was mixed with 30/70 chitosan/n-HA composite powder at P/L (powder/liquid) ratio of 1 g/ml, and then the obtained paste was processed into specimens with a size of $\Phi 6 \times 1$ mm. After being dried at room temperature, the weight of these specimens was marked as W_0, and then were immersed in 30 ml SBF for 1, 2, 4 and 8 weeks at 37 °C. After soaking, the specimens were removed from the fluid, gently rinsed with deionized water for 5 times and cleaned with filter paper to get rid of water on the surface, and then weighed and marked as W_1. After being dried, the specimens were weighed again and noted as W_2. The rate of weight loss (L) was calculated according to the equation of $L = (W_0 - W_2)/W_0$, and the rate of water adsorption (A) was determined by the equation of $A = (W_1 - W_2)/W_2$. The surface microstructures and crystal phases of these specimens after soaking were analyzed by scanning electron microscope (SEM) and XRD. Calcium concentrations in the SBF solutions were measured as a function of soaking time with inductively coupled plasma atomic emission spectroscope (ICP).

3. Results

3.1. Burn-out test

Burn out test was often used to confirm the actual composition of organic/inorganic composites [7]. Table III lists the theoretical and experimentally determined

TABLE III Theoretical and actual compositions of chitosan/n-HA composites as determined by burn-out tests at 800 °C

Theoretical chitosan/n-HA composition		Actual chitosan/n-HA composition					
		%Chitosan			%n-HA		
%Chitosan	%n-HA	S I	S II	S III	S I	S II	S III
20	80	20.23	20.17	20.30	79.77	79.83	79.70
30	70	30.15	29.87	29.94	69.85	70.13	70.06
40	60	39.86	39.92	40.13	60.14	60.08	59.87
50	50	49.97	50.35	50.29	50.03	49.65	49.71
60	40	61.03	61.58	59.95	38.97	38.42	40.05
70	30	70.89	68.95	71.23	29.11	31.05	28.77

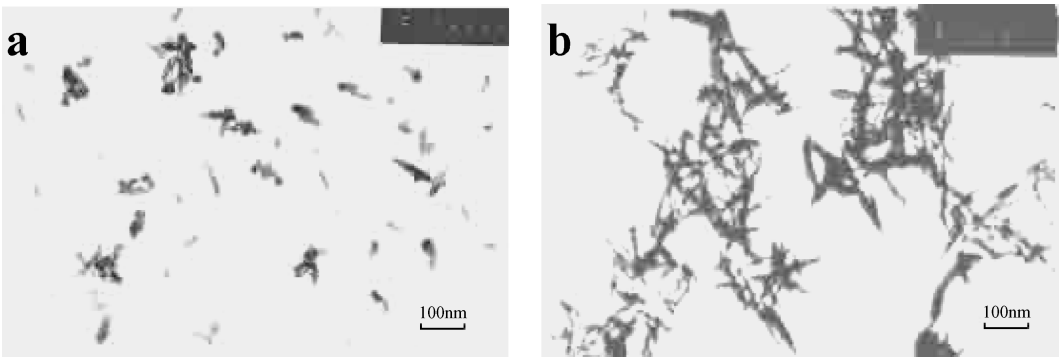

Figure 1 TEM photographs of (a) pure n-HA and (b) 20/80% chitosan/n-HA composite.

compositions of the composites, the samples are sintered in air at 800 °C for 2 h. It can be seen that the actual compositions are very close to the theoretical values. Moreover, different parts of the same composite have almost identical composition, which indicates that the two phases disperse into each other uniformly. In addition, the burn out of pure chitosan sample in air at 800 °C gives almost no residue while the pure n-HA results in 8.7% decrease in weight. Therefore, the observation should be taken into account when calculating the compositional values of various chitosan/HA composites.

3.2. TEM observation

TEM photographs of n-HA and chitosan/n-HA composite are shown in Fig. 1. Fig. 1(a) is that for n-HA synthesized in ambient condition and Fig. 1(b) is for chitosan/n-HA composite prepared by co-precipitation method. It can be seen from the photographs that the n-HA powder exhibits nanometer rod crystals with a mean size of about 30 nm in length and 10 nm in width, and these n-HA crystals have a good dispersive property and display a relatively uniform morphology. With the addition of chitosan, the chitosan/n-HA powders show a slimly shuttle-like morphology with an average size of about 80 nm in length and 20 nm in width. This infers that the growth of n-HA crystals in the (002) direction of *c*-axis may have been promoted.

3.3. IR analysis

IR spectra of chitosan, pure n-HA, as well as chitosan/n-HA composites are given in Fig. 2. In addition to the characteristic PO_{4-}^{3-} and OH-derived bands as well as adsorbed water bands, CO_3^{2-}-derived bands at 874 cm^{-1} and around 1420–1480 cm^{-1} are also observed in Fig. 2(a). The spectrum in Fig. 2(g) of pure chitosan displays an absorption at 1655 cm^{-1}, which represents the amide I carbonyl stretching as the shoulder on the amine deformation peak at 1599 cm^{-1}[21]. However, the two peaks were shifted to lower wavenumber when chitosan was mixed with n-HA, as shown in Fig. 2(b)–(f). Comparing these IR patterns, it can be seen that the specific peaks of both pure n-HA and pure chitosan all appear in the spectra of chitosan/n-HA composites except for slight band-shifts and peak-decrease.

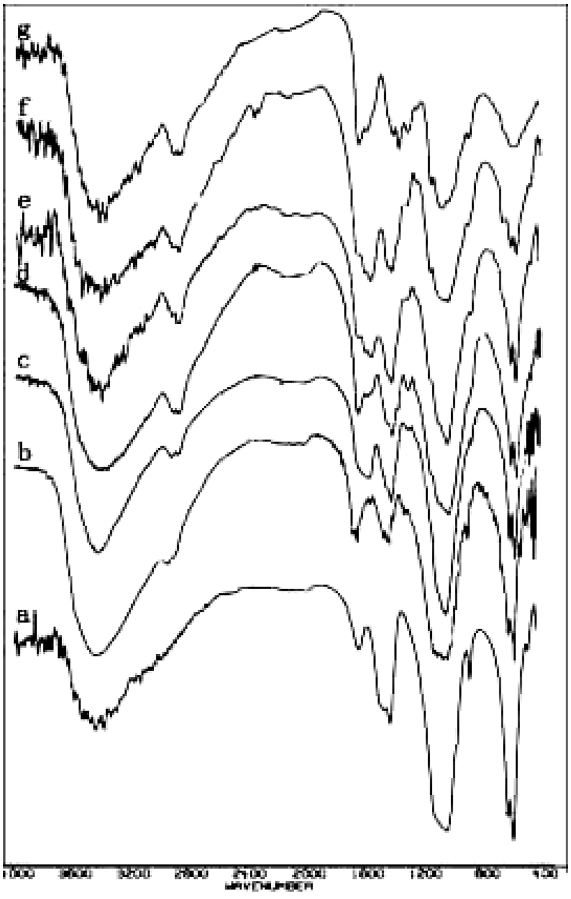

Figure 2 IR spectra of (a) pure n-HA, and chitosan/n-HA composites with weight ratios of (b) 20/80% (c) 30/70%, (d) 50/50%, (e) 60/40% and (f) 70/30%, and (g) pure chitosan.

3.4. XRD measurement

Fig. 3 shows the X-ray diffraction patterns for pure n-HA, chitosan and their composites with different weight ratios. The characteristic peaks for n-HA are detected in the spectrum, as shown in Fig. 3(a). However, the broadening diffraction peaks indirectly prove that the synthetic n-HA is composed of small crystals that are poorly crystalline and nonstoichiometric. In Fig. 3(g), two main diffraction peaks of chitosan at $2\theta = 10^\circ$ and 20° are observed. All these chitosan/n-HA composites as shown in Fig. 3(b)–(f), are characterized by specific diffraction peaks arising from n-HA and chitosan. However, the relative intensity of specific peaks for chitosan decreases evidently with the increase of n-HA content in these composites.

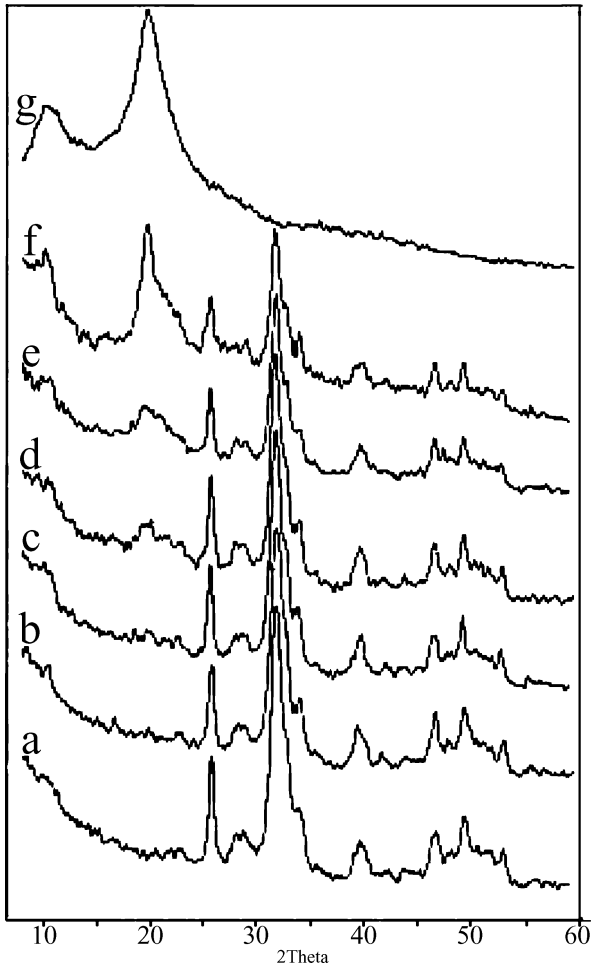

Figure 3 XRD patterns of (a) pure n-HA, and chitosan/n-HA composites with weight ratios of (b) 20/80% (c) 30/70%, (d) 50/50%, (e) 60/40% and (f) 70/30%, and (g) pure chitosan.

3.5. Compressive strength

Table IV illustrates changes in the compressive strength with the increase of chitosan fraction in the composites. It is obvious that the compressive strength firstly increases with the content of chitosan and then reaches a maximum value, about 120 MPa, corresponding to the composite with weight ratio of 30/70, and after that the strength begins to decrease.

3.6. SEM observation

Fig. 4 shows the microstructures of the specimens after soaking in SBF solutions at 37 °C for 0, 1, 4 and 8 weeks. For the specimen before soaking (Fig. 4(a)), n-HA particles imbedded uniformly in the organic chitosan and a comparatively dense structure can be observed. After one-week soaking (Fig. 4(b)), it can be seen that many tiny HA particles deposited on the surface of the specimen and some pores formed. Four weeks later (Fig. 4(c)), more particles attached on the surface and the specimen showed a porous structure; until 8 weeks, much more particles deposited and piled up on the surface and covered part of these pores.

3.7. XRD patterns after soaking

Fig. 5 shows XRD profiles for the specimens after soaking in SBF for 0, 1, 2, 4, and 8 weeks. It is obvious that the specific diffraction peaks for chitosan disappeared little by little with the soaking time and the intensity of HA diffraction peaks, however, increased gradually.

3.8. The rates of weight loss and water adsorption

From Fig. 6, it can be seen that the rate of weight loss firstly increases with soaking time and reaches a maximum at the forth week, and then decreases. The similar trend is also found on the rate of water adsorption as a function of soaking time, which is shown in Fig. 7.

3.9. Calcium concentration

Calcium concentration in the SBF solution as a function of soaking time is shown in Fig. 8. An abrupt decrease of calcium concentration occurred in the first week, and after that, followed by a continuous slow decrease.

4. Discussion

Studies on the organic-inorganic materials system have been carried out for a long period, but the miscibility of the two phases is a noteworthy problem for the blend research [7, 18]. However, it is desirable that chitosan/n-HA composite in the present study has an excellent miscibility in various weight ratios and no phase-separation shows up in these blends. Burn-out test also confirms that n-HA particles are almost perfectly incorporated into the composites and there is a good uniformity between the two phases. In chitosan/n-HA composite, when the content of chitosan is higher, the minute n-HA particles as filling phase are dispersed into the continuous organic matrix uniformly, but with the decrease of chitosan, the organic phase is not enough to encapsulate n-HA crystals and just acting as a glue bond these grains together homogeneously.

TABLE IV Changes of compressive strengths with the composition of chitosan/n-HA composites

Theoretical Chitosan/n-HA composition		Compressive strength	Theoretical Chitosan/n-HA composition		Compressive strength
%Chitosan	%n-HA	(MPa)	%Chitosan	%n-HA	(MPa)
20	80	101.67	50	50	86.87
30	70	119.86	60	40	85.56
40	60	108.92	70	30	66.64

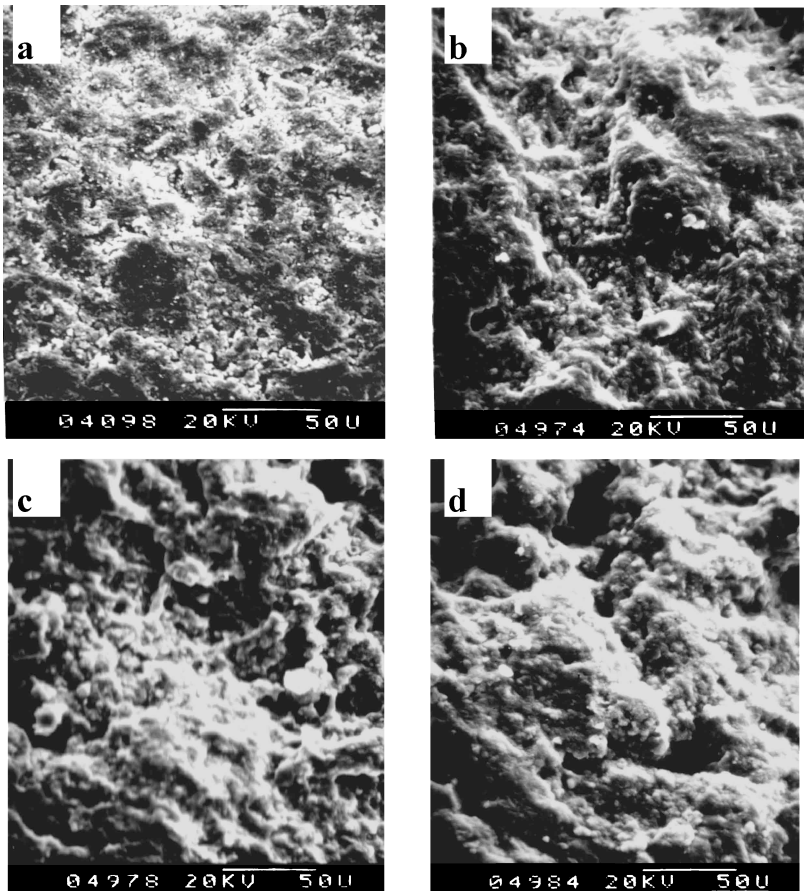

Figure 4 SEM images of specimens after soaking in SBF solutions for (a) 0 week, (b) 1 week, (c) 4 weeks and (d) 8 weeks. Magnification ×400.

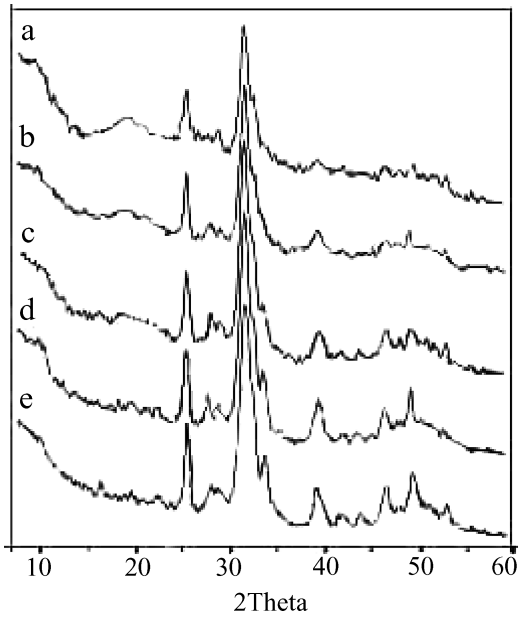

Figure 5 XRD patterns of specimens after soaking in SBF solutions for (a) 0 week, (b) 1 week, (c) 2 weeks, (d) 4 weeks and (e) 8 weeks.

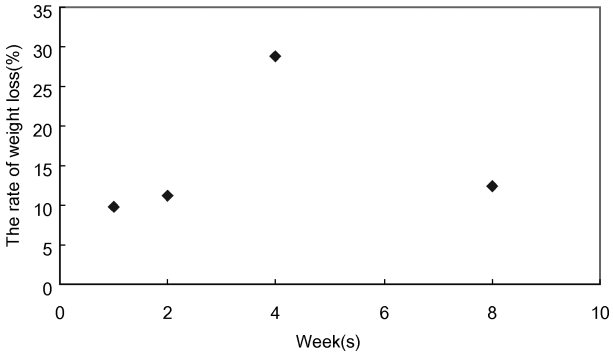

Figure 6 The rate of weight loss as a function of soaking time.

Chitosan is characterized by forming chitosan-metal complexes in which metal ions coordinate with amino groups of chitosan [19, 20]. During the process of co-precipitation, the instantaneous precipitation of chitosan encloses the n-HA grains inside polymer fibers. It has been reported that the *c*-axis of HA crystals tends to align along the chitosan fibers [21]. Therefore, a close relationship is found between the adjacent Ca ($d_{Ca} = 0.344 \times 3 = 1.03$ nm) ions of HA and adjacent amino groups of chitosan (1.03 nm) [22]. So, it is possible that several amino groups are involved in the formation of apatite crystals. IR spectra show that the two characteristic bands of amide I (1655 cm^{-1}) and amide II (1599 cm^{-1}) shift to lower wavenumber after being compounded, which suggests that interaction must take place between chitosan and n-HA, including hydrogen bonds between $-NH_2$ and $-OH$ of n-HA as well as the chelation between $-NH_2$ and Ca^{2+}. The more these bands shift to lower wavenumber, the stronger the hydrogen bonds between these groups, and also the stronger the interaction between these molecules.

Among the composites studied, the 30/70 chitosan/n-HA exhibits the maximum value of compressive strength, about 120 MPa, which is strong enough to be used in load-bearing sites of bone tissue. In contrast,

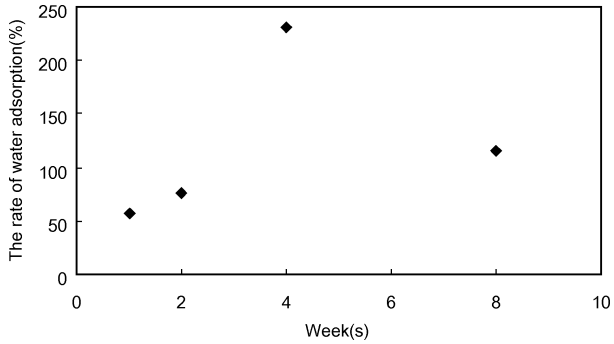

Figure 7 The rate of water adsorption as a function of soaking time.

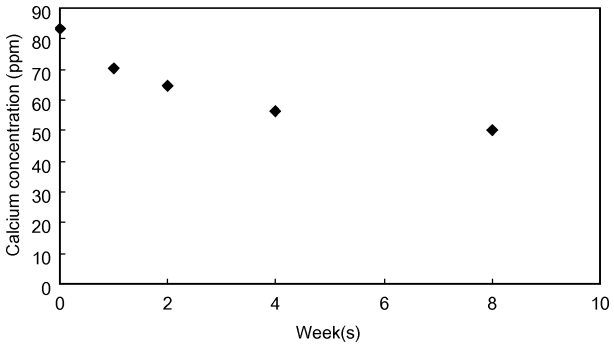

Figure 8 Calcium concentration in SBF solutions as a function of soaking time.

the compressive strength of pure HA compact prepared by the similar method has been reported as 6.5 MPa [23], about one twentieth of the maximum value of the composite. In general, the proper stress transfer occurring between the reinforcement and the matrix governs the mechanical characteristics of filled polymers [18, 27]. As to the present study, chemical and mechanical interlocking between n-HA and chitosan accounts for the efficient stress-transfer in the composite system. Besides, the interactions such as hydrogen bonding and chelation between the two phases, also contribute to the good mechanical properties of chitosan/n-HA composite.

From SEM photos, it can be known that chitoan in the composite gradually degraded during the soaking in SBF solution, which resulted in plenty of macro- and micro-pores on the surface of and inside the specimens. At the same time, a lot of tiny apatite crystals deposited on the surface of the specimens, and till the 8th week, a thin layer of bone-like apatite, being highly bioactive, was formed. At the first 4 weeks, the degradation rate of chitosan was higher than the deposition rate of apatite on the surface of specimens, which corresponding to a continuous increase of the rate of weight loss. After that, the deposition of apatite is prior to the degradation of chitosan, so the rate of weight loss decreased. This was also confirmed by the rate of water adsorption. With the degradation of chitosan during the specimen's soaking in SBF solution, a more sponge-like structure was formed, which can hold more water. However, with more apatite crystals deposition, some of these pores were filled or covered, so water adsorption decreased.

From Fig. 5, it can be observed that, with the increase of specimens' soaking time, the specific peaks at $2\theta = 10^\circ$ and $2\theta = 20^\circ$ for chitosan gradually decreased and almost disappeared after 8 weeks. Whereas the intensity of the specific peaks for HA increased little by little during the same process. The content of chitosan in specimens reduced with its degradation, which made the diffraction peaks for chitosan very faint and almost undetectable. On the other hand, the degradation of chitosan made more n-HA particles expose out and thus induced more apatite crystals to deposit, which was reported by Z. Young *et al.* [24]. Therefore, the intensity of diffraction peaks for n-HA was strengthened. The changes of calcium concentration in SBF solutions further confirmed that the composite is enough bioactive to induce bone-like apatite to deposit on the surface when being immersed in SBF solutions.

When the chitosan/n-HA composite implanted in body using as tissue scaffold, the degradation of chitosan makes room for the growth of new bone and then is substituted by new bone completely. It has been reported that chitosan can promote nucleation and growth of apatite and calcite crystals as well [25]. Moreover, the surface of chitosan is hydrophilic, which can facilitate cell adhesion, proliferation and differentiation [26]. So the chitosan/n-HA composite, used as bone substitutes, are hopeful to activate the regeneration and remodeling of bone tissue.

5. Conclusion

In the paper, a series of chitosan/HA composites have been fabricated by a co-precipitation method. The HA in these composites was poorly crystalline carbonated nanometer crystals. There is an excellent miscibility between chitosan and n-HA and no phase-separation has been observed. Stronger interactions between the two parent phases have occurred, which endows these composites with good mechanical strength. The maximum compressive strength was about 120MPa corresponding to the 30/70 chitosan/n-HA composite. *In vitro* tests shows that degradation of chitosan in the 30/70 composite has taken place and a layer of bone-like apatite has formed on the surface of the composite, which indicates that the composite has high bioactivity. Owing to these excellent properties, chitosan/n-HA composites have extensive potentials to be used as scaffold materials in bone tissue engineering and will contribute to the guided regeneration of new bone.

Acknowledgment

This study was funded by the Ministry of Science and Technology of China.

References

1. L. YUBAO, J. DE WIJN, C. P. A. T. KLEIN, S. VAN DE MEER and K. DE GROOT, *J. Mater. Sci.: Mater. Med.* **5** (1994) 252.
2. L. YUBAO, Z. XINGDONG and K. DE GROOT, *Biomaterials* **5** (1994) 263.
3. L. S. WOJCIECH, S. PAVEL, B. KULLAIAH, E. R. RICHARD, S. T. KEVOR and F. J. VICTOR, *ibid.* **23** (2002) 699.

4. B. DEFNE and T. A. CUNEYT, *J. Europ. Ceram. Soc.* **19** (1999) 2573.
5. R. V. SNYDERS, B. L. EPPLEY, M. KRUKOUESKI and J. J. DELFINO, *J. Oral. Macillofac. Surg.* **51** (1993) 517.
6. I. YAMAGUSCHI, K. TOKUCHI, H. FUKUZAKI, Y. KOYAMA, K. TAKAKUDA, H. MONMA and J. TANAKA, *J.Biomed. Mater. Res.* **55** (2001) 20.
7. B. J. MEENAN, C. McCLOREY and M. AKAY, *J. Mater. Sci.: Mater. Med.* **11** (2000) 48.
8. K. MASANORI, I. SOICHIRO, I. SHIZUKO, S. KENICHI and T. JUNZO, *Biomaterials* **22** (2001) 1705.
9. W. R. WALSH, J. HARRISON, A. LOEFLER, T. MARTIN, D. VAN SICKLE, M. K. BROWN and D. H. SONNATEND, *Clin. Orthop.* **375** (2000) 258.
10. Z. YONG and Z. MIQIN, *J. Non-Crys. Sol.* **282** (2001) 159.
11. J. V. PAMELA, W. T. M. HOWARD, P. D. STEPHEN, M. LOIS, W. BIN and H. W. PAUL, *J. Biomed. Mater. Res.* **58** (2002) 585.
12. M. FWU-LONG, T. YU-CHIUN, L. HSIANG-FA and S. HSING-WEN, *Biomaterials* **23** (2002) 181.
13. I. MASAYUKI, O. KATSUAKI, S.YOSHIO, Y. HIROFUMI, H. HIDEMI, M. TAKEMI and K. AKIRA, *Int. Cong. Ser.* **1223** (2001) 251.
14. W. LISHAN, K. EUGENE, W. AILEEN and L. LEE YONG, *J. Biomed. Mater. Res.* **63** (2002) 610.
15. V. M. SUNDARARAJAN and W. T. M. HOWARD, *Biomaterials* **20** (1999) 1133.
16. S. VIALA, M. FRECHE and J. L. LACOUT, *Ann. Chim. Sci. Mat.* **23** (1998) 69.
17. A. DOMARD, *Int. J. Biol. Macromol.* **9** (1987) 98.
18. G. S. SAILAJA, S. VELAYUDHAN, M. C. SUNNY, K. SREENIVASAN, H. K. VARMA and P. RAMESH, *J. Mater. Sci.* **38** (2003) 3653.
19. K. OGAWA and K. OKA, *Chem. Mater.* **5** (1993) 26.
20. N. C. BRAIER and R. A. JISHI, *J. Mol. Struct. (Theochem)* **499** (2000) 51.
21. Y. ISAMU, I. SOICHIRO, S. MASUMI, O. AKIYOSHI and T. JUNZO, *Biomaterials* **24** (2003) 3285.
22. I. YAMAGUCHI, K. TOKUCHI, H. FUKUZAKI, Y. KOYAMA, K.TAKAKUDA, H. MONMA and J. TANAKA, *J. Biomed. Mater. Res.* **55** (2001) 20.
23. K. HIROTAK, *Biomed. Mater. Res. Far East (I). Kyoto: Kobunshi Kankokai Inc.* (1993) 35.
24. Z. YONG and Z. MIQIN, *J. Biomed. Mater. Res.* **55** (2001) 304.
25. R. A. A. MUZZARELLI, G. BIAGINI, A. DEBENEDITTIS, P. MENGUCCI, G. MAJNI and G. TOSI, *Carbon. Polym.* **45** (2001) 35.
26. Z. YONG and Z. MIQIN, *J. Biomed. Mater. Res.* **61** (2002) 1.
27. W. XIAOHONG, M. JIANBIAO, W. YINONG and H. BINGLIN, *Biomaterials* **22** (2001) 2247.

Received 29 January
and accepted 12 August 2004